Highlights

Synthetic generation of vibroacoustic modulation signals for structural health monitoring

Benjamin Boll, Lennart Dorendorf, Peter Oppermann, Erik Willmann, Bodo Fiedler, Bernd-Christian Renner, Marcus Rutner, Robert Horst Meißner

- Generation of VAM from static ultrasonic measurements for a robust and independent SHM.
- Decoupling VAM from actual ambient vibration makes measurements comparable over time.
- Data reduction of 99.99 % compared to traditional VAM evaluation.
- Feasible with undersampled signals resulting in reduced hardware requirements.
- Enabling the application of VAM for actual structures.

Synthetic generation of vibroacoustic modulation signals for structural health monitoring

Benjamin Boll[a,b], Lennart Dorendorf[c], Peter Oppermann[d], Erik Willmann[a], Bodo Fiedler[a], Bernd-Christian Renner[d], Marcus Rutner[c], Robert Horst Meißner[a,b]

[a]*Institute of Polymers and Composites, Hamburg University of Technology, Germany*
[b]*Institute of Surface Science, Helmholtz-Zentrum Hereon, Geesthacht, Germany*
[c]*Institute for Metal and Composite Stuctures, Hamburg University of Technology, Germany*
[d]*Institute for Autonomous Cyber-Physical Systems, Hamburg University of Technology, Germany*

Abstract

The vibroacoustic modulation (VAM) is a nonlinear ultrasonic testing method that utilizes the modulation of a high-frequency/low-amplitude probe wave with a low-frequency/high-amplitude pumping vibration, resulting in high sensitivities to damages in the structure. However, applying the method outside of the laboratory as a structural health monitoring system for actual structures is challenging, since the amplitude and frequency of the ambient vibrations—which is ideally utilized as pumping vibration—fluctuates over time. To circumvent this, we present a synthetic generation of the VAM signal using only the probe measurements , acquired at two (or more) stress levels of the structure when a steady state is reached. We could show that only 16 values (8 measured values of only two stress levels with a sampling

Email address: benjamin.boll@tuhh.de/robert.meissner@tuhh.de (Robert Horst Meißner)

frequency of 1/20 of the Nyquist frequency) are required to generate the often calculated Modulation Index with a mean deviation of 0.97 % to the expected dynamic measured values for glass fiber reinforced composites and 1.86 % for the aluminum specimens, which is negligible compared to a typical increase of the Modulation Index of 10–30 dB in case of severe damage. Even undersampled measurements at each stress level can be used without sacrificing accuracy, which reduces the sensing requirements for the sensor nodes. Moreover, this method decouples VAM from the actual need for a constant recurrent frequency and amplitude of the natural vibration in order to reliably compare measurements throughout the lifetime. Hence, this work aims to open the possibility of ultimately applying VAM to assess the structural health of complex structures.

Keywords: Damage Detection, Vibroacoustic Modulation, Structural Health Monitoring, Nondestructive Testing, Nonlinear Acoustics, Lamb Waves

1. Introduction

The evaluation of structural integrity is a concern for all engineering applications. Hence, Non-Destructive Testing (NDT) is crucial for reliable operations. Within the multitude of NDT methods, especially nonlinear ultrasonic methods attain high sensitivities for small defects, which often remain concealed in linear ultrasonic methods. [1] A highly sensitive nonlinear technique is the Vibroacoustic Modulation (VAM) analysis, which has been the subject of first studies in the 1990s [2, 3, 4, 5, 6, 7], recent publications [8, 9, 10, 11, 12, 13, 14, 15, 16, 17, 18, 19] and many more in between. The

method utilizes the modulation of a high-frequency ultrasonic Lamb wave as a carrier (or probe) signal $s_{\mathrm{c}}(t)$ with a high-amplitude pump vibration $s_{\mathrm{p}}(t)$ for which an already present ambient signal or an artificially generated wave can be utilized. VAM has been applied to many applications, from monitoring fatigue crack growth in aluminum specimens,[20, 21, 22, 23] detection of impacts and delaminations in composite structures [24, 25, 26] or identification of adhesive contaminations. [26, 27, 28] A comprehensive review of already tested materials and promising applications is given by Pieczonka *et al.*[29] and in the book chapters [30, 31]. Unfortunately, most research on VAM has been performed exclusively on laboratory-scale specimens where both vibrations (pump and carrier) are artificially introduced. Especially the pump wave, which is enabling the high sensitivity of VAM, is particularly identified and optimized [32], or even the full data of a freqeuncy sweep over a range is used.[33] Hence, the utilization of VAM in many works could be classified as an NDT method rather than the Structural Health Monitoring (SHM) method it could become.

To monitor and estimate the structural health of large civil or engineering structures, the excitation of a defined pump vibration is cumbersome and requires powerful actuators. However, these actuators depend on strong external energy sources and therefore prevent easy integration of the VAM into the structure. Therefore, it would beneficial to use already existing environmental vibrations. For optimal damage detection and the possibility of damage localization [19], data has to be acquired at several locations with a network of multiple sensors. Therefore, the optimal placement of sensors,[34] and a wireless application of energy harvesting sensor nodes for data mea-

surement and transmission are relevant and actively developed. [35, 36, 37] However, the required energy consumption for the high-frequency excitation, high sampling rate measurements, complex computational evaluation, and the transmission of results pose severe difficulties for VAM applications on large structures. Using the short-time Fourier-transform (STFT) on a highly undersampled signal has shown great potential to reduce the energy for the measurement and data evaluation. [38] Nevertheless, the VAM method—as applied up to now—requires the excitation of an ultrasonic signal s_c and the ambient vibration s_p to be constant during the measurement and more importantly for the following measurements as well. However, such ideal pump vibrations are not evident in actual civil or engineering structures. Vibrational data acquired at the Köhlbrandbrücke in Hamburg (Germany) shows that the ambient vibration is a superposition of frequencies in the range 10–20 Hz. [38, 39] Additionally, these ambient structural vibrations depend on many environmental influences, e.g., winds, temperature, traffic, and seasonal aspects. Hence, the eigenmodes and resulting dominant frequencies in the structure fluctuates, which influences the pump vibration and hampers the applicability of VAM.

To overcome these limitations, we present a new method to acquire the data for the VAM method. The novelty of this work is the artificial reconstruction of a VAM signal from several measurements of only the carrier vibration at different stress states of the structure, instead of analyzing the carrier and pump vibrations simultaneously. The method is based on the assumption that the carrier frequency is much higher compared to the pump frequency and hence, requires only a few periods T_c of the ultrasonic carrier

s_c at these stress levels. These carrier measurements are combined into a synthetic signal, from which the damage state can be assessed, for example, with the conventional Modulation Index (MI) [40] or other evaluation methods. [29, 38] The presented method is the first which actively decouples the VAM analysis from the amplitude and frequency of the pump wave. Hence, the damage state could be assessed, even if the ambient conditions change. The synthetic VAM increases the comparability for a reliable and precise health monitoring. Ultimately, the presented procedure leads to a significant data reduction of each measurement, thus reducing the requirements on the sensor nodes possibly enabling a more sophisticated multi-sensor VAM approach in the future which is even able to locate damages.

2. Methodology

2.1. Vibroacoustic modulation

The VAM analysis is an active acoustic method that utilizes the nonlinear response of the material to detect damages and can be applied to NDT and potentially SHM. Typically, the specimen or structure is excited simultaneously with a low-frequency vibration s_p (often referred to as pump wave) and an ultrasonic vibration s_c (probe or carrier wave). The ultrasonic carrier wave with a frequency of f_c is introduced by piezoceramic actuators attached to the specimen. However, methods for introducing a pump wave s_p with frequency f_p differ in the literature and are either orthogonal or longitudinal excitations. Electromagnetically shakers [23, 41] or piezoceramics [22, 26, 42] typically introduce the wave orthogonal, while servohydraulic testing machines [21, 43, 44, 45] introduce it longitudinal.

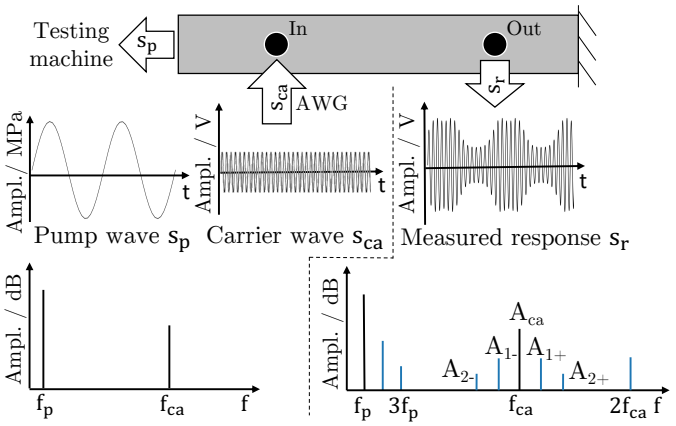

Figure 1: Schematic experiment setup. The pumping wave s_p is introduced by a servo-hydraulic pulsing machine, while the high frequency carrier s_c is generated by a piezoceramic actuators, depicted as black disks and driven by an arbitrary waveform generator (AWG). (adapted from [27])

The pump wave periodically alters the stress state in the specimen. This variation is particularly enhanced around inhomogeneities or defects and periodically affects the propagation of the ultrasonic waves. The system response signal s_r is typically measured by a second piezoceramic or a laser doppler vibrometer. [24, 44, 46] The general approach of a VAM analysis is schematically illustrated in Figure 1. The initiation and growth of a damage alters the stress distribution, which further affects the nonlinear response of the specimen. Consequently, the higher harmonics ($kf_\mathrm{p} \wedge kf_\mathrm{c} \mid k \in \mathbb{N}$) and sidebands around the carrier wave ($f_\mathrm{c} \pm kf_\mathrm{p} \mid k \in \mathbb{N}$) will increase, the latter representing a stronger modulation. [29] These components can be seen in the frequency domain of the measured signal, calculated by a Fast Fourier Transform (FFT). The appearance of sidebands is associated to a clapping mechanism of the defects and changes in the stress distribution around the

tips of the cracks. Ref. 29 associated the highest longitudinal stress of the pump wave with the lowest signal strength in the system response. However, the numerical and experimental results from Dorendorf *et al.*[44] suggest that this assumption is dependent on the excited carrier frequency with regard to the eigenmodes of the specimen. A thorough mathematical explanation of the occurrence of sidebands is found elsewhere. [22, 44, 26, 47, 48, 49]

VAM is commonly evaluated by calculating the ratio of the sideband amplitudes to the carrier amplitude, resulting in the Modulation Index (MI) and given in decibels:[40, 43, 50]

$$\mathrm{MI} = 20 \cdot \log_{10}\left(\frac{A_{-1} + A_{+1}}{2A_\mathrm{c}}\right) \tag{1}$$

Here, A_c is the spectral amplitude of the carrier wave s_c. The sideband amplitudes A_k are differentiated by the numeric index k that indicates its corresponding frequency. A summation or averaging of several sidebands can be performed to extract more information from each measurement. Additionally, averaging over multiple frequencies is commonly suggested to eliminate variations in MI due to resonances and antiresonances of the tested specimen. [7, 27, 43, 45]

Furthermore, the modulation in a VAM measurement of any structure is a superposition of amplitude modulation and angular modulation (phase and frequency) of the frequencies present in the structure and partly caused by a periodic change of wave propagation characteristics due to nonlinearities in wave propagation and the signal path length. Hence, separating the measured signal into different modulation types has shown benefits, as they could be attributed to different types of damage in a sample. [20, 50, 43] Hu *et al.* 50 proposed the separation by the *Hilbert-Huang transformation* and

suggests that the modulated signal amplitude has a higher correlation with the size of the crack. In contrast, Refs. 20 and 43 concluded that applying the *In-phase Quadrature Homodyne Separation algorithm*, the frequency modulation indicates fatigue damage for aluminum specimens at an earlier point. The analytical model of Dorendorf *et al.*[44] indicates the influence of each nonlinearity (e.g. damages, contaminations, among others) on both types of modulation.

Finally, for inspections of large structures, it is beneficial to utilize the ambient vibrations which are already present in the structure and originate from environmental influences (winds, water flow, etc.) or other load factors (traffic, rotor movement, engines, pumps, etc.). [7] The application of these vibrations allows low energy measurements, but also results in multiple unknowns regarding the low-frequency pump vibrations that do not have a constant amplitude and frequency over time. Therefore, it hampers the application of the separation algorithms mentioned above and makes the VAM cumbersome to reproduce for standardized measurements on these large structures.

2.2. Synthetic signal generation

Traditionally, a sinusoidal pump vibration is used to alter the stress in the structure, which widens the cracks periodically and results in signal modulation. It was shown by Dorendorf *et al.*[44], that the measured amplitude modulation of VAM oscillates harmonically between measurements of only the excited carrier at the highest and lowest stress of the pump vibration. For most frequencies, the extreme stresses coincide with either the minimal or maximal measured voltage on the piezoceramics. The amplitude hereby

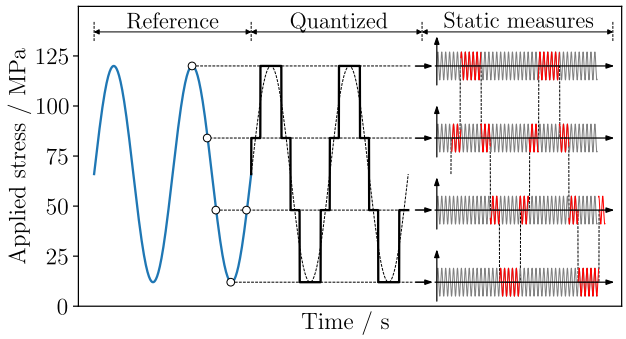

Figure 2: The conventional sinusoidal low-frequency excitation (blue) can be quantized into discrete stress levels (black). The synthetic VAM is composed of measurements from only the high-frequency excitation at each of the stress levels (right). The red areas mark the chunks of each measurement, which are concatenated into the composed synthetic signal.

depends on the evaluated frequency with respect to the eigenmodes of the corresponding specimen.

Since $f_\mathrm{c} \gg f_\mathrm{p}$, it can be assumed that the amplitude of the measured modulated signal at each point in time can be approximated by the steady-state response of the carrier wave s_c at the corresponding stress state. Therefore, the main concept behind the synthetic VAM is to quantize the pump vibration into a distinct number of discrete stress levels n—-similar to analog-to-digital signal processing—and acquire only the high-frequency response at these individual levels σ_l, where l indication actual stress at this level.

This procedure is visualized in Figure 2 for $n = 4$ individual stress levels. The pump vibration—which is traditionally used for VAM—is shown on the left side. The dots on the pump wave indicate the mapped sampling points for the quantization of the pump vibration. In this example, equidistant stress steps were chosen, but even random points can be feasible as well.

The quantized pump wave is shown in Figure 2 (mid) and at each step of this quantization, only the carrier response is measured (right).

The synthetic signal is composed of concatenated signal fragments, extracted from the carrier measurements as defined by the quantized pump vibration (Figure 2 right). Due to the concatenation, this method results in non-continuous transitions between each segment and a resulting quantization error. Intuitively, the quantization error increases with fewer levels n and is explained in more detail later. Furthermore, this method will have a small error due to the assumption that a linear relationship between the strain of the specimen and the amplitude of the vibration is evident, resulting in a pure sinusoidal envelope of the resulting signal. The error in MI, which is the deviation from the expected offset and results of this assumption, will be discussed based on the results of experimentally tested specimens and the results from numerical finite element simulations in the following sections. In Figure 3 (left) the synthetic generation of an amplitude-modulated signal is shown for the two representative numbers of stress levels $n = 2$ and $n = 3$. The pump wave s_p of the amplitude modulation (Equ. A.3 in the Appendix) was quantized to n stress levels at which the carrier signal was computed and the points were extracted to calculate the static cases. Note that the envelope of the modulated signals is almost symmetrical, hence it is irrelevant whether the upper or lower half is shown in this figure.

Amplitude modulation is visible for all synthetic signals and follows the dynamic reference, illustrated as a black envelope. By increasing the number of steps n, the synthetic signal converges towards the dynamic system response. However, the utilization of more steps also comes with the price

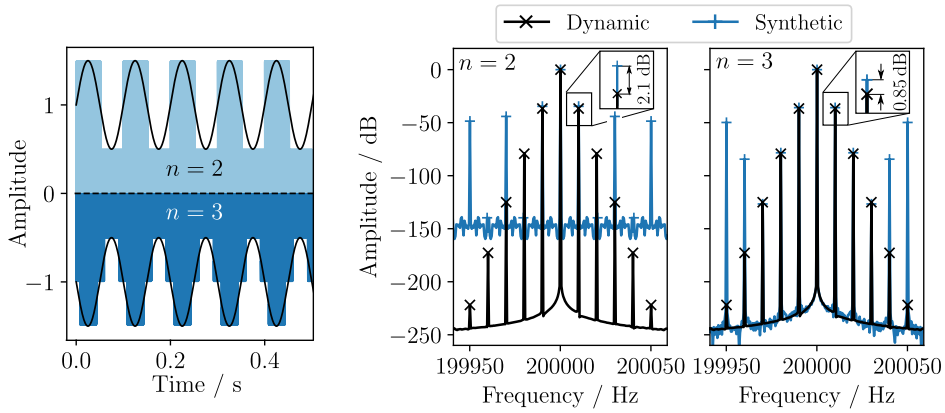

Figure 3: Comparison of an amplitude and phase modulated signal to the synthetic generated signals from $n = 2$ and 3 static levels. The time domain (left) and also the frequency domain (right) show a higher precision of the approximation with an increased n.

of more required measurements and data points, which has to be stored and transmitted. Hence, more relevant for the application of sensor networks is the reduction of steps to the minimum of ($n = 2$), which results in the composition of a square wave (Figure 3, upper left).

The Fourier Transform $\mathcal{F}$ of a composed synthetic signal from only two steps—resulting in a square wave (sq)—shows unique characteristics in the frequency domain (eq. 2) as known from signal processing. [51]

$$\mathcal{F}\left\{\mathrm{sq}(2\pi f_\mathrm{p})\right\} = \begin{cases} \frac{4}{l\pi}, \text{for } |f| = l f_\mathrm{p}, \text{ with } l = 1, 3, 5, \ldots \\ 0, \quad \text{otherwise} \end{cases} \tag{2}$$

Due to the particular nature of square waves, only odd sidebands ($l = 1, 3, 5, \ldots$) appear in the frequency domain, where the first sideband is increased by a factor of $4/\pi$, compared to the dynamic signal response from a sinusoidal pumping wave s_p. Furthermore, the following odd sidebands have the amplitude of $4/(l\pi)$.

If we apply a square wave $s_\mathrm{p} = \mathrm{sq}(2\pi f_\mathrm{p})$ for the signal modulation, the relationship in eq. 2 also applies to the sidebands around the carrier. Hence, the intensity of the carrier is equal for a square modulation and sinusoidal modulation. Consequently, the MI of a synthetic signal from $n = 2$ is offset by $20 \cdot \log_{10}(4/\pi)$, which equals 2.098 dB as shown in the inset of Fig. 3 (right). Although the amplitude of the carrier matches the dynamic signal in both cases, an offset can be seen for the first sidebands of the square signal of the value mentioned above of $4/\pi$. The amplitude of further sidebands decreases linearly (cf. eq. 2). For $n = 3$, the synthetic signal closely resembles the dynamic measurement, resulting in a high similarity of the first three sidebands in the frequency domain.

Most intuitively, VAM depends on the sampling rate f_s, which directly influences the maximal measurable frequency. Nyquists theorem states that the sampling rate should minimally be $f_\mathrm{s} > 2 \cdot f_\mathrm{max}$. For VAM measurements, f_max represents the frequency of the highest sideband that should be evaluated. There are already some techniques (e.g., undersampling of the measured signal[38]) to overcome this boundary and reduce the data size of the measured signal. However, these methods presume ideal conditions for the measurement, a sinusoidal vibration of the structure of a constant amplitude, which is cumbersome for the evaluation of large structures.

The second parameter is the time of measurement, which influences the resolution of the FFT and, therefore, how precise the sidebands are represented. Ideally, longer measurement times increase the resolution and hence the robustness of the data acquisition. However, this is only valid for an ideally generated modulation. The variant conditions of real applications

require the measurements to be timed at recurring conditions. Hence, retrieving as much information as possible from only short signals is relevant for applying VAM outside the laboratory.

If we assume an ideal periodic signal, a traditional VAM has to be measured over a full period T_p of the low-frequency to include all information. For this measurement, the frequency and, more importantly, the amplitude of the low frequency should closely match the prior measurements for comparable results. However, the synthetic VAM can be generated from only one period T_c of the high-frequency of each stress level n. Since $f_\mathrm{c} \gg f_\mathrm{p}$, the measurement times can be reduced significantly, resulting in much less data to be saved and transmitted. Furthermore, the measurements can be performed at defined stress states. Hence, the overall amplitude only has to surpass the defined measurement stresses to achieve comparable VAM measurements, independent of the actual frequencies present in the structure.

Generation of a synthetic signal is explained by using data chunks from the steady-state measurement with a sampling rate above Nyquist's theorem. Since a steady-state of the carrier at each stress measurements is assumed, the carrier of a defined frequency can be recreated from just a few points. Since the frequency is defined by the exciting piezoceramics, only the amplitude and phase of the mean-centered sine must be determined. Hence, a minimum of $p = 2$ measurement points would be sufficient to approximate the steady-state sine and create a synthetic signal with an arbitrary length. [52] By increasing the number of points p, a sine can be fitted to the measurement or more sophisticated methods such as STFT can be applied to calculate these values with a higher tolerance to noise, resulting in higher precision.

Consequently, downsampling of the existing measured signals was performed by selecting every 10th or 100th value in order to mimic signals sampled at $f_\mathrm{s} = 200\,\mathrm{kHz}$ or even $f_\mathrm{s} = 20\,\mathrm{kHz}$ which is less than 0.05 of the dedicated Nyquist rate.

Since one of the main goals of this paper is to demonstrate the possibilities a synthetic VAM computation offers over performing dynamic VAM, the shown experimental results stem from $p = 8$ measured points of the high-frequency measurements s_c at the levels σ_l. Furthermore, we evaluate the difference between using the original signal and a signal downsampled by a factor of 100 (i.e. $f_\mathrm{s} = 20\,\mathrm{kSa/s}$).

2.3. Specimen manufacturing and testing

Two types of specimens were produced and tested experimentally to validate the proposed synthetic VAM. Two aluminum open-hole tension specimens were made in accordance to the work of Dorendorf *et al.*[44] and Oppermann *et al.* [38] and similar to the specimen tested by Ramezani. [43] They were cut from a cold-pressed aluminum 7075 plate with a hole of 4.5 mm diameter, drilled in the center. The dimensions are shown in the upper half of Figure 4.

Additionally, two specimens were made from a glass fiber reinforced polymer laminate (GFRP) in a cross-ply layup that has been manufactured in a resin transfer molding process. Dry UT-E500 E-glass fibers (Gurit) were arranged in a $[0, 90_3]_\mathrm{s}$ layup and impregnated with a low-viscosity epoxy system (RIMH135 and RIMR137 from Hexion). The plate was cured at 50 °C for 24 h, and post-cured for 15 h at 80 °C outside the mold in compliance with the datasheet. The fully cured plates were cropped to the specified dimensions

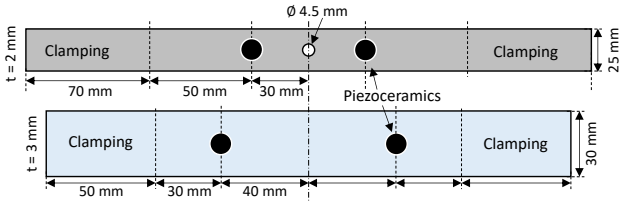

Figure 4: Dimensions and positioning of the piezoceramics for the aluminum (upper) and GFRP $[0, 90_3]_s$ specimens (lower).

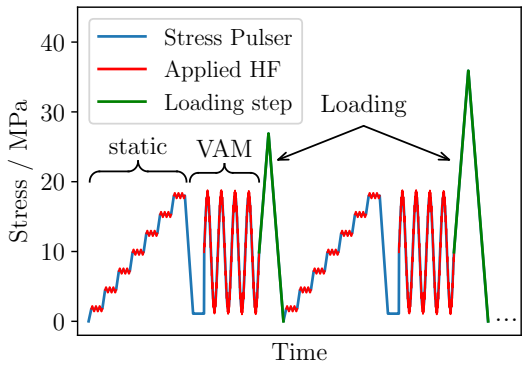

Figure 5: Method of testing to compare the conventional VAM and the synthetically created VAM, combined from the shown static measurements. The blue curve depicts the applied stress with the pulsing machine, and the red curve indicates when the high frequency is excited.

with a water-cooled corundum saw blade (ATM Brillant 265). Afterwards, the cutting surface was polished with 1000-grit sandpaper to reduce crack initiations from the edges to a minimum. Vibroacoustic measurements and specimen tests were performed for both materials on a servo-hydraulic testing machine (Instron) with a loading capacity of 40 kN and controlled by the Instron WaveMatrix^{TM} software. Due to different material properties, failure mechanisms, and specimen types of the two materials, the testing strategy was slightly adapted for each material. For the aluminum specimen, a fa-

tigue loading was tested in the tension-tension regime with a maximal stress of $\sigma_{\max} = 150\,\mathrm{MPa}$, a fatigue frequency of $f_{\mathrm{fatigue}} = 5\,\mathrm{Hz}$ and a stress ratio of $R = \frac{\sigma_{\min}}{\sigma_{\max}} = 0.1$ to achieve a lifetime of approximately 30 000 cycles. Prior to the fatigue loading, and after every 2000 cycles, a conventional dynamic VAM ($\sigma_{f_{\mathrm{p}}} = 3 - 30\,\mathrm{MPa}$) was performed. Additionally, the high-frequency vibration was measured for three static loads ($\sigma_{\mathrm{static}} = 3,\ 16,\ 30\,\mathrm{MPa}$) to compare the synthetic VAM with the conventional method. The process was repeated until the failure occurred. Aluminum specimens were tested over their lifetime to evaluate whether the synthetic VAM can track the damage state and MI of a metallic structure.

For the GFRP specimen, increasing loads were applied stepwise to introduce defects to the material. When reaching the so-called "knee-stress" of a cross-ply laminate, matrix cracks in between the 90° fibers occur (inter-fiber failure), resulting in a decreased Young's modulus. Hence, after each conventional VAM ($\sigma_{f_{\mathrm{p}}} = 2.2 - 22\,\mathrm{MPa}$) and the static measurements for the synthetic VAM ($\sigma_{\mathrm{static}} = 2.2, 5.6, 8.9, 12.2, 15.6, 18.9, 22\,\mathrm{MPa}$), a uniaxial tensile test was performed with a load increase of 5 MPa/s until the defined stress in the specimen was reached. Subsequently, the maximal load was increased until multiple cracks occurred in the specimen, enabling to derive a correlation between the number of cracks in the FRP specimen and the conventional and synthetic VAM results. The measurement procedure is illustrated for the GFRP specimens in Figure 5.

The high-frequency carrier s_{c} of all specimens was introduced and measured with piezoceramic actuator disks (PIC255, 10 x 2 mm from PI-Ceramics) which were applied to the specimen by double-sided tape (Tesa 56172). Com-

pared to a 2k-adhesive, the vibrations excited in the specimen and, consequently, the voltages measured at the receiving piezoceramic are reduced due to the adhesive tape, resulting in a slightly increased signal-to-noise ratio. However, the overall information quality is comparable, while the adhesive tape makes the actuators reusable.

To excite the piezoceramic actuators and perform the data acquisition, a NI-USB 6366 data acquisition board (National Instruments) was used with a sampling rate of $f_\mathrm{s} = 2\,\mathrm{MSa/s}$. Controlled by Matlab, the generated signal from the NI was twofold amplified (BUF634 with an additional low-pass of 420 kHz) to a $12\,\mathrm{V_{pp}}$ sine. The carrier frequency was determined as the range of the strongest response in a linear frequency sweep between 1–300 kHz. Since the resulting modulation depends on several conditions, as summarized by Lim *et al.* [22], a frequency range of $f_\mathrm{c} = 185 - 215\,\mathrm{kHz}$ was chosen. In this range, 61 carrier excitation frequencies $f_\mathrm{c}$have been measured with a spacing of 500 Hz. For all specimens, the dynamic VAM measurements were acquired for a duration of 2 s, and the static measurements for 1 s. Data with sampling rates below $f_\mathrm{s} = 2\,\mathrm{MSa/s}$ are generated by selecting the signal at every 10th or 100th value.

3. Results and Discussion

Before validating the synthetic VAM algorithm with actual measurements, a proof of concept was conducted on a signal in which the amplitude and phase were modulated simultaneously. For both modulations (see eq. A.3 for AM and A.4 for PM in the Appendix), the modulating term $\cos(\omega_\mathrm{p} t + \phi_\mathrm{p})$ is quantized into n steps, where n was increased from

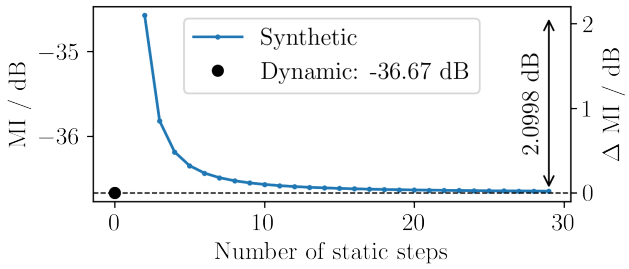

Figure 6: The MI of the synthetic signal converges with an increasing number of steps to the MI of the dynamic measurement.

$2 \leq n \leq 30$. For every n, the MI was calculated from the static measurements and compared to the dynamic result. The resulting FFT for $n = 2$ has already been shown (Figure 3) and was related to the nature of square waves. As expected, the MI of the synthetic square wave is offset by $20 \cdot \log_{10}(4/\pi) = 2.098\,\mathrm{dB}$ compared to the dynamic VAM. Increasing the number of quantization steps results in convergence to the MI of the dynamic signal, as shown in Figure 6. Also the higher-order sidebands converge towards the values found in the dynamic measurements and could be used for further evaluations.

In the following, our synthetic method is applied to GFRP and aluminum specimens to compare the resulting modulation to the dynamic VAM that is traditionally used. The damage was introduced into the GFRP specimens with subsequent tensile testing at increasing loads, and the resulting cracks were quantifiable by eyesight. Therefore, both methods can be easily compared and related to the number of cracks. VAM measurements below the "knee-stress"—which indicates inter-fiber damage of a cross-ply laminate—were performed to acquire a baseline. When the specimen was loaded with a tensile stress of 56 MPa, the "knee-stress" was surpassed and first inter-fiber cracks appeared. The amount of cracks after each loading cycle is shown

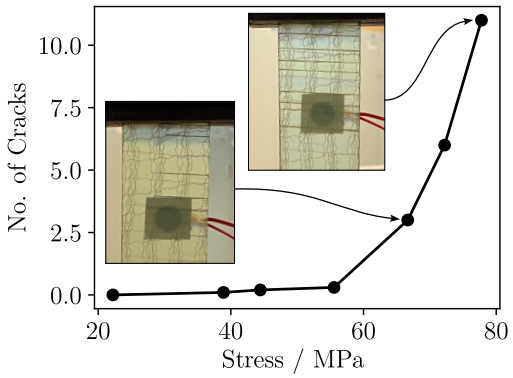

Figure 7: Number of cracks in the 90° layer after each uniaxial loading of the GFRP specimen. The specimen with the manifestation of the cracks is illustrated after two loadings.

in Figure 7. In the insets of Figure 7, depicting two different states of the specimen, the severity and density of inter-fiber cracks is visible by darker horizontal lines. Note that the first cracks after 56 MPa penetrated the specimen's 90° layers only over half the width but evolved into full cracks at the next stress level of 69 MPa.

Figure 8 (left) compares the measured vibrations with a carrier frequency of $f_c = 185\,\text{kHz}$ before and after a damage is introduced into the specimen. Note that the measured signals are almost symmetrical. Therefore, the differences between the synthetic signals are shown for $n = 2$ in the upper half and $n = 3$ in the lower half. To further illustrate the synthetic process, the signal chunks of the different stress levels are differentiated by color.

As expected, the maximal and minimal amplitudes of the dynamic measurements coincide with the amplitudes of the static measurements. When comparing the amplitudes with respect to the damage and stress, the measured voltage at a stress of 120 MPa is higher compared to the stress state

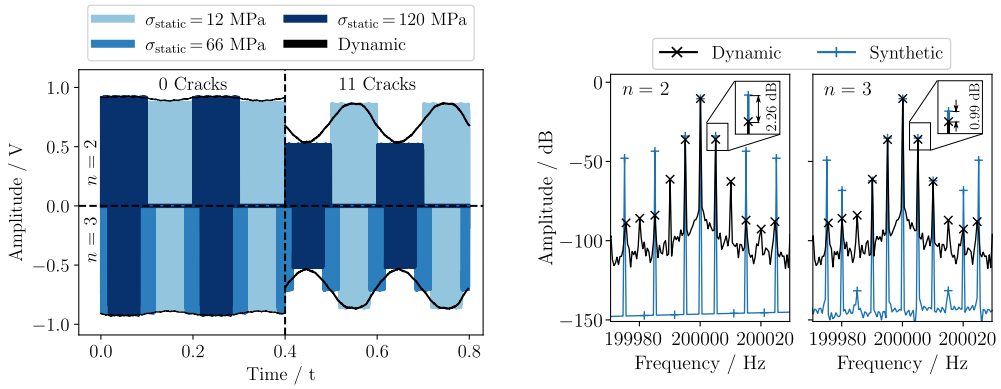

Figure 8: Synthetic generated signals (left) of a GFRP specimen from $n = 2$ (upper) and $n = 3$ (lower) static measurements for the pristine state compared to 11 cracks. The envelope of the dynamic VAM is given as black line. For $n = 2$ and $n = 3$ the frequency spectrum of the synthetic and dynamic VAM is compared (right). The insets show the enlargement of the first sidebands with the mean deviation of this specimen.

of 12 MPa for the undamaged specimen. However, this proportion at the shown frequency reverses after introducing a few cracks. Interestingly, the measured amplitude at the low stress of 12 MPa stays constant, whereas the amplitude at the higher stress is significantly reduced due to the cracks. This observation is in accordance with the often-mentioned bi-linear stiffness behavior explaining a VAM by a stress-related crack opening. However, there are also frequencies (f_c =194 kHz) where the amplitude at the higher stress state remains constant, while the measured voltage at 12 MPa is decreased. This duality supports and underlines the physical explanation of VAM given by Dorendorf *et al.*,[44] which states that the maximal and minimal amplitude of the modulated signal s_r can coincide with either the highest or lowest stress. The amplitude of the carrier depends on whether the ratio between carrier frequency and the natural frequency f_c/f_{eigen} is greater than or less

than one and, hence, which eigenmode is primarily contributing to the system response. Moreover, a phase shift occurs between the alternating and combined signal fragments, which, as a result, also incorporates angle modulation into the synthetic method. As before with the amplitude modulation, the change in phase appears stepwise, resulting in shifted values compared to those of the dynamically modulated phase.

Figure 8 (right) illustrates the frequency domain around f_c for both synthetic signals compared to the dynamic measurement. The results are in accordance with observations made for ideal modulated signals, as shown in Figure 3 (right). For $n = 2$, the first sidebands are offset from the dynamic signal by about $\Delta\mathrm{MI} = 2.1\,\mathrm{dB}$ which is reduced to $\Delta\mathrm{MI} = 0.85\,\mathrm{dB}$ for the three-step signal. Although the higher-order sidebands of the two-step signal behave according to eq. 2, the three-step synthetic VAM also approximates the second sidebands with reasonable accuracy by reducing the quantization error. The disagreement of the third and further sidebands could be improved by computing the synthetic VAM for more stress levels.

The differences between a synthetic and dynamic MI are shown in Figure 9 for three synthetic signals with $n = 2, 3, 7$ and a range of carrier frequencies. The synthetic VAM was generated from 8 points of a signal sampled at $f_\mathrm{s} = 2\,\mathrm{MSa/s}$. As expected, the MI is offset compared to the dynamic measurements, which mainly results from the synthetic generation itself. Using only two static measurements $n = 2$ results in a mean offset of $\Delta\mathrm{MI}_2 = 2.254 \pm 0.45\,\mathrm{dB}$, which is close to the expected offset of $\Delta\mathrm{MI}_{2,\mathrm{ref}} = 2.098\,\mathrm{dB}$. Therefore, there is a mean error of $0.154\,\mathrm{dB}$, which can be expressed as $0.73\,\%$ compared to the mean dynamic MI. This off-

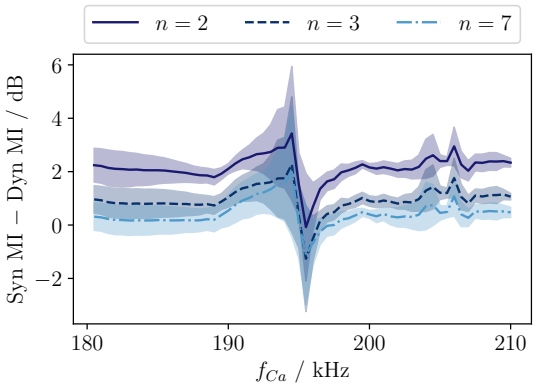

Figure 9: Deviation of the synthetic MI compared to the conventional measurement. Shown are the mean error and its standard deviation of all tensile loadings. Note that the error is the deviation from the expected offset, which for $n = 2$ is $\Delta\mathrm{MI}_{2,\mathrm{ref}} = 2.01\,\mathrm{dB}$.

set can be reduced by using $n = 3$ or even $n = 7$ static stress levels to $\Delta\mathrm{MI}_7 = 0.44 \pm 0.44\,\mathrm{dB}$ for the synthetic signal generation. Hence, the error is reduced to 0.12 %, which underlines the relevance of this method. More results are given in Table B.2 *ff.* of the Appendix. Furthermore, Figure 9 indicates, that the mentioned errors result mainly from two frequency ranges around the resonances, which are at 196 kHz and 205.5 kHz for all n and result in a minimal modulation. This can be seen in the SI (Figure 1), where the MI is plotted across the entire frequency spectrum. Interestingly, the synthetic MI on the left flank of the resonance around 196 kHz is significantly increased and on the right side of the resonance decreased. By choosing a suitable frequency range between 180–190 kHz deviations are reduced. It should be mentioned that the areas around the resonances are also commonly avoided for evaluating a conventional VAM in the literature or compensated for by averaging over a frequency range, as proposed by several

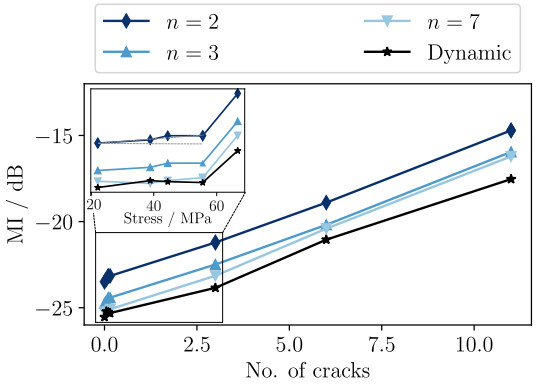

Figure 10: In the GFRP cross-ply laminate, the averaged MI increases linearly with each inter-fiber crack. The mean MI over all measured frequencies for a synthetic signal with various steps (2,3,7) is compared to the dynamic measurement. The inset, shows the same graphs plotted over the max. applied stress, to separate the first four measurements before the first inter-fiber crack appeared, to highlight the increase in MI with each subsequent loading.

publications. [7, 23]

When averaging the entire frequency range, the MI increases almost linearly with every new inter-fiber crack in the specimen, as shown in Figure 10 for the dynamic measurement and synthetic signals. Interestingly, the synthetic MI evolves more linearly. The synthetic MI is able to robustly detect cracks in GFRP specimen and the difference between the synthetic and dynamic MI is negligible compared to the modulation increase per crack. Furthermore, there is an increase in MI even before the first inter-fiber crack was detected, as enlarged in the inset of figure 10. This increase could indicate some first microcracks in the composite or damages due to the clamps of the testing machine. However, the increase in MI due to the first inter-fiber cracks is significantly higher. All values for the different number of levels

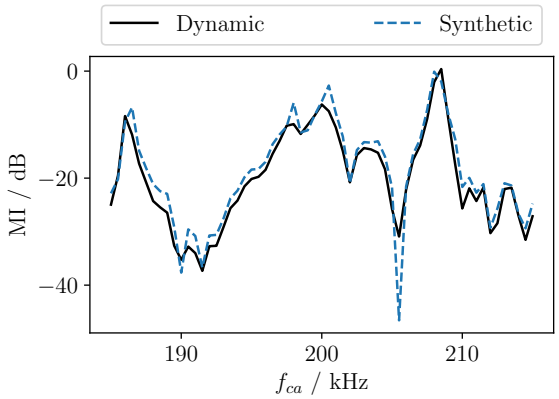

Figure 11: MI of an aluminum specimen (2) after ten thousand fatigue cycles. The dynamic measurement (continuous) is compared to the synthetic computation (dashed).

n, the used sampling frequency f_s, and the number of points used p can be found in the Appendix in Table B.2.

The results of the second GFRP specimen are closely comparable to the presented ones. The deviations are minimally different with an error of 0.97 % for $n = 2$. Further values can be found in Table B.3.

Compared to the tested GFRP specimens, the MI of aluminum specimens fluctuates over 30 dB across the measured carrier frequencies, resulting from more pronounced resonances in the material. A comparison between a synthetic ($n = 2, f_\mathrm{s} = 2\,\mathrm{MSa/s}, p = 8$) and dynamic MI after ten thousand fatigue cycles is shown in Figure 11. Similarly to the GFRP specimen, the highest deviations occur in the vicinity of the extremes of either weak or severe modulations (e.g., 206.5 kHz) and result in a slightly increased error from -1.3 to -1.9 %. However, these errors (around 0.34 dB) are neglectable compared to the MI increase of 10–30 dB which is shown in literature [20, 38] as a result of a relevant damage. The mentioned mean deviations and errors

Table 1: Mean deviation and its standard deviation of the tested specimen generated from each $p = 8$ points of $n = 2$ static load levels.

Specimen	Mean deviation	Mean error	
	[dB]	[dB]	[%]
GFRP 1	2.254 ± 0.447	0.154	0.73
GFRP 2	2.302 ± 0.418	0.202	0.97
Aluminum 1	1.828 ± 1.329	-0.272	-1.26
Aluminum 2	1.761 ± 0.804	-0.339	-1.86

are summarized in Table 1 and all values can be found in Table B.4 and B.5.

The frequencies with a large error, which occur in the vicinity of minimal or maximal modulation, can be explained by inspecting the raw signal. Here, the assumption of a quasi-linear change in wave propagation due to the periodically altered stress is no longer valid, resulting in signals with a non-sinusoidal envelope.

3.1. Distorted envelope functions

Besides the near-ideal MI concordance between synthetic and dynamic measurements in most cases, we have found frequencies where the synthetic method differs from the expected offset. In these cases, the envelope function of the resulting dynamic signal s_r does not have a nearly sinusoidal form. As suggested by Dorendorf *et al.*,[44] the steady-state dynamic magnification factor of a damped oscillation model—which is proportional to the amplitude acquired in our experiments—depends on the excitation frequency in relation to the natural frequencies (and modes) of the system. Due to the periodical applied stress in VAM, the natural frequencies of the specimen are

periodically shifted, resulting in a periodically changed dynamic magnification factor. In the vicinity of these natural frequencies, or exactly between two of them, the dynamic magnification factor behaves strongly nonlinear over one period of the low frequency T_p. Hence, the envelope function of the measured response s_r exhibits more than two extreme values during that period T_p.

Figure 12 shows a numerical system response of an aluminum specimen which was modeled with the finite element software Abaqus CAE and is demonstrating this phenomenon. The model's geometry is equivalent to the tested aluminum specimens and the modeling details are described in more detail in the work of Dorendorf *et al.*[44], who has validated the results experimentally using a 3D scanning laser vibrometer (PSV 500-3D-M, Polytec) The model's parameters are also given in Table C.6 of the Appendix. The specimen's longitudinal displacement obviously influences the out-of-plane acceleration, which is proportional to the measured voltage, i.e. signal, at a piezoceramic in the prior mentioned experiments. The periodically applied stress results in a severe amplitude modulation of the simulated acceleration. Note that the steady-state amplitudes fit the envelope function at the defined stress with negligible error even for frequencies, where the minimum value of the envelope function does not coincide with the minimal or maximal stress level. As explained in the previous sections—when employing synthetic VAM—it is assumed that the envelope function is near sinusoidal with the minimum and maximum values coinciding with min or max stress or vice versa. Intuitively, when calculating the synthetic VAM ($n = 2$) on these types of signals, the error increases.

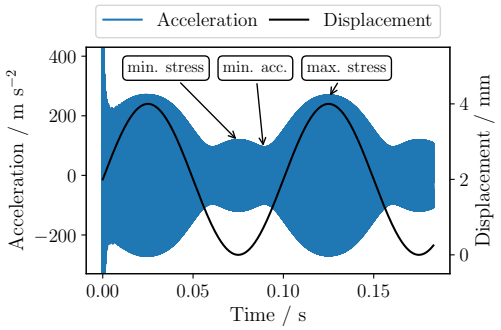

Figure 12: FE simulation of an aluminum specimen with a periodically applied elongation (black line). For certain carrier frequencies ($f_c = 210\,\text{kHz}$, $f_p = 10\,\text{Hz}$) the minimal amplitude of the response (blue) is not coinciding with the minimal elongation. (Adapted from [44])

In the shown example, the difference is $\Delta\text{MI}_2 = 1.68\,\text{dB}$ and further explains the areas of high errors in the vicinity of the resonance frequencies (i.e 196 kHz & 205.5 kHz) in Figure 9.

Averaging the MI over a frequency range—as proposed in many publications—minimizes the error due to these frequencies. Furthermore, increasing the number of levels n reduces this error.

3.2. General application for data-reduction

Finally, the possibility of further reducing hardware requirements is addressed, as data reduction is crucial to the deployment of many sensor nodes to monitor the structural health of large structures with VAM. The most relevant work in this regard is the application of undersampling by Oppermann *et al.*[38], where a data reduction of $88 - 99.8\,\%$ was achieved compared to a Nyquist-based sampling rate. The lower bound of 88 % was calculated for the work of Ooijevaar *et al.* [53] who used a pumping frequency of 1455 Hz

and a carrier frequency of 50 kHz. Since the greatest common divisor of both frequencies is relatively small, the undersampling method requires a higher sampling rate, resulting in a lower data reduction. For experiments with frequencies similar to our work, Oppermann *et al.* could reduce the number of measurement points by 99.8 %. With the STFT algorithm applied on a dynamic undersampled VAM measurement, the MI deviates $\Delta\mathrm{MI} = 0.1668\,\mathrm{dB}$ on average, compared to the traditional evaluation. These remaining 0.2 % of the undersampled data still result in 1600 points over a time period of 2 s for which a constant vibration of the structure is assumed. Especially the condition of constant vibration over this time and between the measurements hinders the application of undersampling in actual structures.

In contrast, our presented method, the synthetic VAM, is capable of significantly reducing the number of required points further. For the conducted experiments with pumping frequencies of 5 Hz and the carrier frequency of $180 - 215\,\mathrm{kHz}$, only $3 - 8$ measured points are needed of at least two stress levels, resulting in a deviation over all frequencies of 0.202 dB for the GFRP and $-0.339\,\mathrm{dB}$ for aluminum. To evaluate the dynamic VAM, at least 0.2 s sampled at 500 kSa/s are needed, which results in 100 000 data points per measurement and subsequently a reduction of 99.984 %.

Moreover, with the synthetic method, we can apply the STFT algorithem or a basic upsampling method to the static measurements acquired at a sampling rate much smaller than the excited carrier frequency. This allows for reduced hardware requirements or possible integrations into existing SHM systems. To showcase this opportunity, the original static measurements for the synthetic VAM were downsampled by a factor of 100 resulting in a

sampling frequency of $f_s = 20\,\mathrm{kSa/s}$ which is far below the carrier frequency f_c. From eight consecutive points of these downsampled signals, a sine with the original sampling rate is recreated and used for the synthetic process. Since this fitting process is already applied, even when the original sampling rate is used, no further adaptations to the method itself had to be performed. With these eight points and $n = 2$, the error of this method is marginally affected and remains below 0.23 dB for the GFRP specimens and 0.34 dB for the aluminum specimens. So there is still potential to further decrease the required samplingrate.

4. Conclusion

The objective of this work was to explore a new approach to measure the vibroacoustic modulation in large structures, where the measurement conditions are not as ideal and constant compared to laboratory tests with one distinct pump frequency of a defined amplitude. To measure the vibroacoustic modulation in large structures, the present ambient vibrations are ideally utilized as low-frequency vibration s_p and only the high carrier wave s_c is excited by a piezoceramic. However, it is a cumbersome endeavor, because these vibrations fluctuate in terms of their frequency and amplitude due to the changes in service loads, traffic, and winds. Measured vibrations from e.g. the Köhlbrandbrücke(Hamburg, Germany) demonstrate this and manifest rather in a frequency range (2–20 Hz) than in a single frequency.

To overcome these shortcomings of VAM for industrial applications, we propose a new synthetic generation of the signals. It is demonstrated that Lamb wave measurements of less than a millisecond, acquired at several static

stress levels, which were interpolated and combined into a synthetic signal are sufficient to robustly approximate the MI and hence detect damages. Moreover, we provide an analysis on how many static stress levels and how many points of the steady state measurement are actually needed in order to achieve an acceptable deviation from the dynamic VAM signal.

To synthetically generate more than just the carrier and first sidebands, more than two static stress levels are needed for the synthetic method. Further validations could be beneficial, since our reference value—the dynamically measured MI—is a measured quantity as well and is affected by the machine and measurement settings. However, in the case of the GFRP specimen, the synthetically generated MI follows the number of cracks more linearly than a dynamic MI.

With the proposed approach, the data size of each measurement is reduced significantly. Only 8 points of each level (which is less than 0.016% of data points compared to the conventional methodology) are required. Consequently, the energy needed to process the data and the bandwidth required to transmit the data is significantly reduced and further enables the deployment of a self-sufficient sensor network. Hence, the effort and costs of monitoring hardware could be significantly decreased. Furthermore, we have shown that the needed sampling rate for the measurements at each stress level could be reduced by magnitudes below the carrier frequency, while still resulting in sufficient accuracy. Thus, the sensor nodes require lower processing speeds and less energy for data acquisition.

This work paves the way and sets the ground for the following material tests and a deployment in larger and more complex structures. We are con-

vinced that the individual measurements at several combined static stress states contain the same information as could be extracted from a dynamic VAM measurement. Since the traditional dynamic approach faces the problem of deviations in frequency and amplitude of the pump vibration over time, the synthetic approach is an expedient extension to the VAM method. Hence, robust measurements of the structural health are in reach, regardless of the changing environmental and loading conditions of the structure.

Conflict of interest

The authors declare that they have no known competing financial interests or personal relationships that could have appeared to influence the work reported in this document.

Funding Statement

This work has been supported by the agency for science, research and gender equality of the city of Hamburg (BWFG, Behörde für Wissenschaft, Forschung und Gleichstellung), the Hamburg University of Technology, and the Helmholtz-Zentrum Hereon in Geestacht (Germany). The funding from the German Research Foundation (DFG) (project number 457416916) is very much appreciated.

5. Data Availability

All data is stored on a secure server at the Institute of Polymer and Composites, Hamburg University of Technology. The raw data, the python codes for processing and the processed data required to reproduce these findings are available from the corresponding author on reasonable request.

Appendix A. Types of signal modulation

To clarify the synthetic process, and test it with ideally modulated signals, the different types of signal modulations which can be present in the VAM signal are presented. A VAM measurement can be the superposition of amplitude modulation (AM) and angular modulation, which can be further divided into frequency modulation (FM) and phase modulation (PM). Let the signal of the ultrasonic carrier wave be defined as

$$s_{\mathrm{c}}(t) = A_{\mathrm{c}} \cdot \sin(\omega_{\mathrm{c}} t) \tag{A.1}$$

and the pumping wave introduced by the hydraulic pulsing machine as

$$s_{\mathrm{p}}(t) = A_{\mathrm{p}} \cdot \cos(\omega_{\mathrm{p}} t + \phi_{\mathrm{p}}) \tag{A.2}$$

with $\omega = 2\pi f$, the individual frequencies $f_{\mathrm{p}} \ll f_{\mathrm{c}}$ and A as amplitude. Then, an amplitude-modulated signal can be combined to

$$\begin{aligned} S_{\mathrm{AM}} &= \left[1 + \frac{s_{\mathrm{p}}(t)}{A_{\mathrm{c}}}\right] s_{\mathrm{c}}(t) \\ &= \left[1 + m_a \cos\left(\omega_{\mathrm{p}} t + \phi_{\mathrm{p}}\right)\right] A_{\mathrm{c}} \sin\left(\omega_{\mathrm{c}} t\right). \end{aligned} \tag{A.3}$$

The amplitude modulation parameter $m_{\mathrm{a}} = A_{\mathrm{p}}/A_{\mathrm{c}}$ expresses the ratio from the amplitudes of the pumping wave to the carrier wave.

In contrast to the AM, both angular modulations are closely related, as shown in the following equations. A phase modulation between the given signals can be expressed as:

$$S_{\mathrm{PM}} = A_{\mathrm{c}} \sin\left(\omega_{\mathrm{c}} t + m_{\mathrm{p}} \cos\left(\omega_{\mathrm{p}} t\right) + \phi_{\mathrm{p}}\right) \tag{A.4}$$

and the frequency modulation, since $s_{\mathrm{p}}(t)$ is a sinusoidal as:

$$S_{\mathrm{FM}} = A_{\mathrm{c}} \sin\left(\omega_{\mathrm{c}} t + \frac{m_f}{\omega_{\mathrm{p}}} \cdot \sin\left(\omega_{\mathrm{p}} t\right) + \phi_{\mathrm{p}}\right). \tag{A.5}$$

Here, m_p is the phase modulation parameter, and m_f is the frequency modulation parameter. When comparing (A.4) and (A.5) it can be concluded that PM is shifted by $\pi/2$ which in addition to multipath propagation through a specimen hinders a separation of FM and PM in an angular modulated signal.

Appendix B. Results for the synthetic recreation of the tested specimens

In the following, four tables are presented, in which the MI generated by the synthetic VAM for different numbers of quantization levels n, sampling frequencies f_s, and the number of points p is compared to the dynamic measurements. The label of each table is the name of the specimen. Since the specified deviation is expected to have an offset, the corrected deviation is calculated by subtracting the analytically calculated value. The specified error percentage is determined by dividing the corrected deviation by the mean value of the MI in the frequency range.

Appendix C. Simulation parameter

The simulation was carried out with the finite element software Abaqus CAE. The model's geometry is equivalent to the tested aluminum specimens

Table B.2: Specimen: GFRP 1

n	f_s [kSa/s]	p	Mean deviation [dB]	Error [dB]	[%]
2	2000	8	2.254 ± 0.447	0.154	0.73
2	2000	50	2.257 ± 0.448	0.157	0.74
2	20	8	2.256 ± 0.449	0.156	0.73
2	20	50	2.257 ± 0.447	0.157	0.74
3	2000	8	0.988 ± 0.438	0.138	0.61
3	2000	50	0.990 ± 0.437	0.140	0.63
3	20	8	0.989 ± 0.441	0.139	0.62
3	20	50	0.991 ± 0.436	0.141	0.63
7	2000	8	0.437 ± 0.439	0.027	0.12
7	2000	50	0.439 ± 0.437	0.029	0.12
7	20	8	0.438 ± 0.438	0.028	0.12
7	20	50	0.439 ± 0.437	0.029	0.13

and the modeling details are described in more detail in the work of Dorendorf *et al.*[44] in Chapter 4. The phenomenon of several modes influencing the signal envelope of the shown signal is already discussed in Fig. 14 of the mentioned publication.

References

[1] T. Kundu, Nonlinear ultrasonic and Vibro-acoustical techniques for Nondestructive evaluation, Springer, 2018. doi:10.1007/

Table B.3: Specimen: GFRP 2

n	f_s [kSa/s]	p	Mean deviation [dB]	Error [dB]	[%]
2	2000	8	2.302 ± 0.418	0.202	0.97
2	2000	50	2.237 ± 0.388	0.137	0.66
2	20	8	2.322 ± 0.488	0.222	1.07
2	20	50	2.326 ± 0.421	0.226	1.08
3	2000	8	1.027 ± 0.348	0.177	0.80
3	2000	50	0.964 ± 0.304	0.114	0.52
3	20	8	1.050 ± 0.404	0.200	0.90
3	20	50	1.052 ± 0.336	0.202	0.92
7	2000	8	0.494 ± 0.314	0.084	0.37
7	2000	50	0.413 ± 0.288	0.003	0.01
7	20	8	0.507 ± 0.365	0.097	0.43
7	20	50	0.500 ± 0.302	0.090	0.40

978-3-319-94476-0.

[2] V. Y. Zaitsev, A. M. Sutin, I. Y. Belyaeva, V. E. Nazarov, Nonlinear Interaction of Acoustical Waves Due to Cracks and Its Possible Usage for Cracks Detection, Journal of Vibration and Control 1 (1995) 335–344. doi:10.1177/107754639500100305.

[3] D. M. Donskoy, A. M. Sutin, Vibro-acoustic modulation nondestructive evaluation technique, Journal of Intelligent Material Systems and Structures 9 (1998) 765–771. doi:10.1177/1045389X9800900909.

Table B.4: Specimen: Aluminum 1

n	f_s [kSa/s]	p	Mean deviation [dB]	Error [dB]	[%]
2	2000	8	1.828 ± 1.329	-0.272	-1.26
2	2000	50	1.909 ± 1.142	-0.191	-0.89
2	20	8	2.154 ± 1.308	0.054	0.25
2	20	50	1.960 ± 1.088	-0.140	-0.65
3	2000	8	0.630 ± 1.365	-0.220	-0.96
3	2000	50	0.727 ± 1.154	-0.123	-0.54
3	20	8	0.955 ± 1.303	0.105	0.47
3	20	50	0.770 ± 1.101	-0.080	-0.35

Table B.5: Specimen: Aluminum 2

n	f_s [kSa/s]	p	Mean deviation [dB]	Error [dB]	[%]
2	2000	8	1.761 ± 0.804	-0.339	-1.86
2	2000	50	1.740 ± 0.805	-0.360	-1.98
2	20	8	1.762 ± 0.795	-0.338	-1.85
2	20	50	1.752 ± 0.775	-0.348	-1.91
3	2000	8	0.492 ± 0.730	-0.358	-1.84
3	2000	50	0.459 ± 0.708	-0.391	-2.00
3	20	8	0.487 ± 0.716	-0.363	-1.86
3	20	50	0.462 ± 0.683	-0.388	-1.99

Table C.6: Material properties of finite elements simulation with Abaqus CAE.

Variable	Variable	Value	
Carrier frequency	f_c	210 000	Hz
Pump frequency	f_p	10	Hz
damping ratio	ξ	0.01	
Rayleigh damping coefficients	α	80	
	β	1.38e-8	
Young's modulus	E	$7{\cdot}10^4$	N/mm^2
Poisson's ratio	ν	0.296	
density	ρ	2752	kg/m^3

[4] A. M. Sutin, D. M. Donskoy, Nonlinear Vibro-Acoustic Nondestructive Testing Technique, Nondestructive Characterization of Materials VIII (1998) 133–138. doi:10.1007/978-1-4615-4847-8-21.

[5] D. M. Donskoy, A. M. Sutin, Vibro-acoustic modulation nondestructive evaluation technique, J. Intell. Mater. Syst. Struct. 3397 (1998) 765–771.

[6] A. E. Ekimov, I. N. Didenkulov, V. V. Kazakov, Modulation of torsional waves in a rod with a crack, The Journal of the Acoustical Society of America 106 (1999) 1289–1292. doi:10.1121/1.427163.

[7] D. M. Donskoy, A. Sutin, A. Ekimov, Nonlinear acoustic interaction on contact interfaces and its use for nondestructive testing, NDT & E International 34 (2001) 231–238. doi:10.1016/S0963-8695(00)00063-3.

[8] S. Miele, P. M. Karve, S. Mahadevan, V. Agarwal, Diagnosis of internal cracks in concrete using vibro-acoustic modulation and machine

learning, Structural Health Monitoring 0 (2022) 147592172110479. doi:10.1177/14759217211047901.

[9] Y. He, Y. Xiao, Z. Su, Y. Pan, Z. Zhang, Contact acoustic nonlinearity effect on the vibro-acoustic modulation of delaminated composite structures, Mechanical Systems and Signal Processing 163 (2022). doi:10.1016/j.ymssp.2021.108161.

[10] T. Yin, C. T. Ng, J. Vidler, V. D. Ho, A. Kotousov, Amplitude-Modulation Vibro-Acoustic Technique for Damage Evaluation, Structural Health Monitoring 0 (2022) 1–22. doi:10.1177/14759217221106209.

[11] X. X. Li, D. Li, W. X. Ren, J. S. Zhang, Loosening Identification of Multi-Bolt Connections Based on Wavelet Transform and ResNet-50 Convolutional Neural Network, Sensors 22 (2022) 6825. doi:10.3390/s22186825.

[12] E. Willmann, B. Boll, M. Scheel, R. H. Meißner, B. Fiedler, Health Monitoring of CFRP laminates under cyclic loading via vibro-acoustic modulation based measurements, Composite Structures 308 (2022) 116696. doi:10.1016/j.compstruct.2023.116696.

[13] D. Liu, D. M. Donskoy, Frequency Modulation in Vibro-Acoustic Modulation Method, Int. J. Civ. Environ. Eng. 17 (2023) 42–47.

[14] A. Alnutayfat, A. Sutin, D. Liu, Vibroacoustic Modulation of Wideband Vibrations and Its Possible Application for Windmill Blade Diagnostics, Int. J. Civ. Environ. Eng. 17 (2023) 31–36.

[15] M. Ehsani, M. Shamshirsaz, M. Sadighi, N. Sepehry, R. Loendersloot, Theoretical and experimental investigations on control parameters of piezo-based vibro-acoustic modulation health monitoring of contact acoustic nonlinearity in a sandwich beam, Appl. Acoust. 203 (2023) 109193. doi:10.1016/j.apacoust.2022.109193.

[16] L. Wei, J. Chen, Determination of optimal probing frequency for enhancing nonlinear vibro-acoustic modulation behaviors of delaminated CFRP based on local defect resonance, Mech. Syst. Signal Process. 187 (2023) 109961. doi:10.1016/j.ymssp.2022.109961.

[17] N. Zhao, L. Huo, G. Song, Vibration acoustic modulation for bolt looseness monitoring based on frequency-swept excitation and bispectrum, Smart Mater. Struct. (2023). doi:10.1088/1361-665x/acb579.

[18] L. Wei, J. Chen, An integrated modeling of barely visible impact damage imaging of CFRP laminates using pre-modulated waves and experimental validation, Compos. Struct. 304 (2023) 116372. doi:10.1016/j.compstruct.2022.116372.

[19] D. Broda, K. Mendrok, V. V. Silberschmidt, L. Pieczonka, W. J. Staszewski, The Study of Localized Crack-Induced Effects of Nonlinear Vibro-Acoustic Modulation, Materials (Basel). 16 (2023) 1653. doi:10.3390/ma16041653.

[20] D. M. Donskoy, M. Ramezani, Separation of amplitude and frequency modulations in vibro-acoustic modulation nondestructive testing

method, Proceedings of Meetings on Acoustics 34 (2018). doi:10.1121/2.0000831.

[21] L. Dorendorf, N. Lalkovski, R. Stolz, M. Rutner, Zuverlässigkeit der Vibro-Akustischen Modulationsmethode zur Strukturüberwachung von Metallen unter Ermüdungsbeanspruchung und ihr Potenzial für das Bauwesen, in: 22. DASt-Forschungskolloquium, Karlsruhe, Deutschland, 2020, pp. 135–139.

[22] H. J. Lim, H. Sohn, Necessary conditions for nonlinear ultrasonic modulation generation given a localized fatigue crack in a plate-like structure, Materials 10 (2017). doi:10.3390/ma10030248.

[23] P. Duffour, M. Morbidini, P. Cawley, A study of the vibro-acoustic modulation technique for the detection of cracks in metals, The Journal of the Acoustical Society of America 119 (2006) 1463–1475. doi:10.1121/1.2161429.

[24] A. Klepka, L. Pieczonka, W. J. Staszewski, F. Aymerich, Impact damage detection in laminated composites by non-linear vibro-acoustic wave modulations, Composites Part B: Engineering 65 (2014) 99–108. doi:10.1016/j.compositesb.2013.11.003.

[25] F. Aymerich, W. J. Staszewski, Experimental study of impact-damage detection in composite laminates using a cross-modulation vibro-acoustic technique, Structural Health Monitoring 9 (2010) 541–553. doi:10.1177/1475921710365433.

[26] B. Y. Chen, S. K. Soh, H. P. Lee, T. E. Tay, V. B. Tan, A vibro-acoustic modulation method for the detection of delamination and kissing bond in composites, Journal of Composite Materials 50 (2016) 3089–3104. doi:10.1177/0021998315615652.

[27] B. Boll, E. Willmann, B. Fiedler, R. H. Meißner, Weak adhesion detection – enhancing the analysis of vibroacoustic modulation by machine learning, Composite Structures 273 (2021) 114233. doi:10.1016/j.compstruct.2021.114233.

[28] B. Boll, E. Willmann, B. Fiedler, R. H. Meissner, Weak-bond detection in single-lap shear bonds by evaluating vibroacoustic modulations with artificial neural networks, in: Proceedings of the 20th European Conference on Composite Materials (Vol 3), volume 3, EPFL Lausanne, Composite Construction Laboratory, 2022, pp. 509–516. doi:10.5075/epfl-298799_978-2-9701614-0-0.

[29] L. Pieczonka, A. Klepka, A. Martowicz, W. J. Staszewski, Nonlinear vibroacoustic wave modulations for structural damage detection: an overview, Optical Engineering 55 (2015) 011005. doi:10.1117/1.oe.55.1.011005.

[30] D. M. Donskoy, Encyclopedia of Structural Health Monitoring- Chapter15 - Nonlinear Acoustic Methods, in: Encycl. Struct. Heal. Monit., 2009.

[31] W. Staszewski, C. Boller, G. R. Tomlinson, Health monitoring of

aerospace structures: smart sensor technologies and signal processing, John Wiley & Sons, 2004.

[32] N. Houhat, V. Tournat, S. Ménigot, T. Boutkedjirt, J. M. Girault, Optimal pump excitation frequency for improvement of damage detection by nonlinear vibro acoustic modulation method in a multiple scattering sample, Appl. Acoust. 155 (2019) 222–231. URL: https://doi.org/10.1016/j.apacoust.2019.06.010. doi:10.1016/j.apacoust.2019.06.010.

[33] Y. Zhang, V. Tournat, O. Abraham, O. Durand, S. Letourneur, A. Le Duff, B. Lascoup, Nonlinear mixing of ultrasonic coda waves with lower frequency-swept pump waves for a global detection of defects in multiple scattering media, J. Appl. Phys. 113 (2013). doi:10.1063/1.4791585.

[34] W. Ostachowicz, R. Soman, P. Malinowski, Optimization of sensor placement for structural health monitoring: a review, Structural Health Monitoring 18 (2019) 963–988. doi:10.1177/1475921719825601.

[35] C. Renner, S. Unterschütz, V. Turau, K. Römer, Perpetual data collection with energy-harvesting sensor networks, ACM Trans. Sens. Networks 11 (2014) 12:1–12:45.

[36] A. H. Alavi, H. Hasni, P. Jiao, K. Aono, N. Lajnef, S. Chakrabartty, Self-charging and self-monitoring smart civil infrastructure systems: current practice and future trends, in: Sensors and Smart Structures Technologies for Civil, Mechanical, and Aerospace Systems 2019, volume 10970, International Society for Optics and Photonics, 2019, p. 109700W.

[37] P. Oppermann, B. C. Renner, Acoustic Backscatter Communication and Power Transfer for Batteryless Wireless Sensors, Sensors (Basel). 23 (2023) 1–26. doi:10.3390/s23073617.

[38] P. Oppermann, L. Dorendorf, M. Rutner, C. Renner, Nonlinear modulation with low-power sensor networks using undersampling, Structural Health Monitoring (2021) 147592172098288. doi:10.1177/1475921720982885.

[39] K. Smarsly, M. Worm, K. Dragos, J. J. P. Abadía, M. Wenner, O. Hahn, Mobile structural health monitoring using quadruped robots, in: Health Monitoring of Structural and Biological Systems XVI, volume 12048, SPIE, 2022, pp. 404–417.

[40] D. Donskoy, A. Zagrai, A. Chudnovsky, E. Golovin, V. Agarwala, Nonlinear vibro-acoustic modulation technique for life prediction of aging aircraft components, Proceedings of the 3rd European Workshop - Structural Health Monitoring 2006 (2006) 251–258.

[41] B. Liu, T. Gang, C. Wan, C. Wang, Z. Luo, Analysis of nonlinear modulation between sound and vibrations in metallic structure and its use for damage detection, Nondestructive Testing and Evaluation 30 (2015) 277–290. doi:10.1080/10589759.2015.1034718.

[42] L. Pieczonka, P. Ukowski, A. Klepka, W. J. Staszewski, T. Uhl, F. Aymerich, Impact damage detection in light composite sandwich panels using piezo-based nonlinear vibro-acoustic modulations, Smart Materials and Structures 23 (2014). doi:10.1088/0964-1726/23/10/105021.

[43] M. Ramezani, Enhancement of Joining Method and Damage Detection Methodology in Structural Materials, Ph.D. thesis, STEVENS INSTITUTE OF TECHNOLOGY, Hoboken, NJ 07030, US, 2018.

[44] L. Dorendorf, N. Lalkovski, M. Rutner, Physical explanation for vibro-acoustic modulation due to local and global nonlinearities in a structure and its experimental and numerical validation, Journal of Sound and Vibration (2022) 116885. doi:10.1016/j.jsv.2022.116885.

[45] A. Alnutayfat, S. Hassiotis, D. Liu, A. Sutin, Sideband Peak Count in a Vibro-Acoustic Modulation Method for Crack Detection, Acoustics 4 (2022) 74–86. doi:10.3390/acoustics4010005.

[46] N. C. Yoder, D. E. Adams, Vibro-acoustic modulation utilizing a swept probing signal for robust crack detection, Structural Health Monitoring 9 (2010) 257–267. doi:10.1177/1475921710365261.

[47] P. Kijanka, R. Radecki, P. Packo, W. Staszewski, T. Uhl, Gpu-based local interaction simulation approach for simplified temperature effect modelling in lamb wave propagation used for damage detection, Smart Materials and Structures 22 (2013) 035014. doi:10.1088/0964-1726/22/3/035014.

[48] A. K. Singh, B. Chen, V. B. Tan, T. E. Tay, H. P. Lee, A theoretical and numerical study on the mechanics of vibro-acoustic modulation, The Journal of the Acoustical Society of America 141 (2017) 2821–2831.

[49] Y. Shen, C. E. Cesnik, Modeling guided wave propagation in composite structures using local interaction simulation approach, in: Structural

Health Monitoring for Advanced Composite Structures, World Scientific, 2018, pp. 47–91.

[50] H. F. Hu, W. J. Staszewski, N. Q. Hu, R. B. Jenal, G. J. Qin, Crack detection using nonlinear acoustics and piezoceramic transducers—instantaneous amplitude and frequency analysis, Smart Materials and Structures 19 (2010) 065017. doi:10.1088/0964-1726/19/6/065017.

[51] E. W. Weisstein, Fourier series–square wave, From MathWorld–A Wolfram Web Resource., ???? URL: https://mathworld.wolfram.com/FourierSeriesSquareWave.html.

[52] J. Alexiou, Describe a sine wave of known frequency with only two points, Mathematics Stack Exchange, 2013. URL: https://math.stackexchange.com/q/383910.

[53] T. Ooijevaar, M. D. Rogge, R. Loendersloot, L. Warnet, R. Akkerman, T. Tinga, Vibro-acoustic modulation–based damage identification in a composite skin–stiffener structure, Structural Health Monitoring 15 (2016) 458–472. doi:10.1177/1475921716645107.